geosciences

MDPI

Article

Preliminary Results of the Kuznetsk Coal Basin Cover Deposits Radon Hazard Assessment

Timofey Leshukov [1,*], Konstantin Legoshchin [1], Elizaveta Baranova [2] and Aleksey Larionov [2]

[1] Department of Geology and Geography, Institute of Biology, Ecology and Natural Resources, Kemerovo State University, 6 Krasnaya Street, 650000 Kemerovo, Russia; geology@kemsu.ru
[2] Department of Genetics and Fundamental Medicine, Institute of Biology, Ecology and Natural Resources, Kemerovo State University, 6 Krasnaya Street, 650000 Kemerovo, Russia; laveivana@mail.ru (E.B.); larionov@kemsu.ru (A.L.)
* Correspondence: tvleshukov@kemsu.ru

Abstract: The study of the influence of geological structure (e.g., faults) on radon emanations is usually applicable provided that there are conditionally background (control) territories with which radon indicators will be compared. In the presented study, we selected an area where pre-Cenozoic faults that could potentially be associated with the radon hazard of the Kuznetsk coal basin were not identified. The cover deposits in the study area are represented by loamy and clayey strata overlying the Paleozoic sedimentary cycles. The radon field was estimated based on the radon flux density (RFD) and radon activity concentration (RAC) in the soil gas. The RAC was measured in two ways—by the sorption method on activated carbon and by the method of active sampling of soil gas from a borehole. At the same time, the role of meteorological conditions and the physical properties of the soil in the radon field was assessed. Our study shows that local variations in the physical properties of the soil are insignificant and do not have a significant effect on the RAC in the soil gas of the Kuznetsk coal basin, with the exception of soil moisture. High values of RAC in the territory considered as conditionally background, in the absence of pre-Cenozoic faults, suggest other causes (the presence of the latest Neogene–Quaternary faults, high concentrations of ^{226}Ra, or other insufficiently studied causes). Due to the absence of faults, it is possible to assume a diffusion type of radon transfer in the geological environment, which indicates a shallow source of radon in such high concentrations. Our results indicate that studies of the ^{226}Ra content and additional studies of the radon hazard of similar areas should also be carried out.

Keywords: soil radon; radon flux density; RFD; radon activity concentration; RAC; soil properties; cover deposits; Kuznetsk coal basin

Academic Editor: Dimitrios Nikolopoulos

Received: 8 November 2024
Revised: 15 December 2024
Accepted: 17 December 2024
Published: 6 January 2025

Citation: Leshukov, T.; Legoshchin, K.; Baranova, E.; Larionov, A. Preliminary Results of the Kuznetsk Coal Basin Cover Deposits Radon Hazard Assessment. *Geosciences* **2025**, *15*, 14. https://doi.org/10.3390/geosciences15010014

1. Introduction

Currently, most countries in the world are making efforts to reduce human exposure to negative environmental factors for the population, thereby reducing the risks of various pathologies, increasing the time of healthy life and life expectancy. One of the problems is reducing the impact of radon [1]. Radon is the second factor in the development of lung cancer, after smoking, with exposure to both factors, and the risks increase synergistically [2,3]. Radon is most dangerous in closed, poorly ventilated rooms, where it can enter from the underlying rocks (geogenic radon) [4–7]. The influence of other sources—building materials [8,9], water, or atmospheric air is, as a rule, comparatively insignificant [10,11], but the building structures themselves can increase the accumulation of radon [5,12]. The

most dangerous is ^{222}Rn, which has the longest half-life of all the isotopes of radon, which allows it to accumulate in environments, including the atmosphere of residential buildings under certain conditions [13]. The role of other isotopes in the general radiation exposure of the population is generally insignificant, and is generally limited to certain geological situations.

^{222}Rn is a decay product of ^{226}Ra, which belongs to the uranium radioactive series, beginning with ^{238}U. Radium is usually found in the upper soil horizons mostly in a weakly mobile form, which makes it an important radiation factor that must be taken into account in engineering and environmental surveys. When radium decays, radon is released into the pore space of soils, where it is sorbed on soil particles, dissolves in water, or migrates due to diffusion, advection, or convection forces. Diffusion forces, caused by differences in radon activity concentrations (RAC) in the soil gas, were considered key to its migration in soils and its transfer to the daylight surface and, accordingly, into residential buildings. Their role was subsequently re-evaluated since the rate and half-life (3.82 days) significantly limit the distance from which it can move. The roles of advective and convective processes have previously been significantly underestimated, but at present they are defined as key ones. High RAC in soil gas cannot be explained by the decay of ^{226}Ra and processes of only diffusion transfer. There are some hypotheses and theories regarding the mechanisms of radon transfer. For example, in some cases, radon emission accompanies the rise of "geogas" from the depths, where radon is transported in the general mixture of gases in the form of "microbubbles" [14–18]. It is known that active tectonic processes leading to a change in the stress–strain state of rocks are capable of changing the transport of radon in the soil gas and stimulating its exhalation to the surface, which is most pronounced in fault zones [19–25]. There is evidence that the temperature difference between the soil air and the surface layer of the atmosphere can stimulate the exhalation of radon to the surface, but at what depth this mechanism operates is a debatable issue [26–30]. It is known about the «chimney effect», which is realized due to the annual cycle of differences in the temperatures of the body of the rock mass and the atmospheric air, as well as differences in temperatures at the foot of mountain slopes and its watersheds. In this case, atmospheric air is capable of transporting radon through permeable zones of the massif [31].

In addition to those listed, there are factors of radon emanation, which also have a significant impact on the RAC and migration of radon in soils. Physical characteristics of the soil, such as density, moisture, and porosity, can reduce the emanation of radon from minerals after the decay of radium, can increase or decrease the possibilities of radon transportation through the pore space of soils, or reduce the sorption of radon on soil particles [32–34]. These examples complement the meteorological factors already described above for the processes of radon migration from the surface layers of soil into the atmosphere.

The diversity of radon migration factors complicates its studies and monitoring in soils, and also affects the forecast of radon-hazardous places and complicates the interpretation of the results. As a result, some factors are often neglected, and attention is focused on the primary predictors. For example, when creating radon geogenic potential (RGP) and geogenic radon hazard index (RGHI) models, a limited set of indicators is used to build models, or only available data are used [35–39]. Some progress in predicting radon hazard is currently being made by machine learning (ML), which is able to take into account a large number of indicators and build quite acceptable forecast maps, but only in the presence of representative data, both in terms of the number of parameters and their spatial representativeness [40–43].

For a comprehensive study of the influence of various geological factors (e.g., faults) on radon transport and exhalation, it is necessary to define conditionally background

(control) territories, with which radon indicators will be compared. In the presented study, we chose an area with no established pre-Cenozoic faults that could potentially be related to the radon hazard of the Kuznetsk coal basin and in which we previously obtained relatively significant RAC in soil gas [44,45]. In addition, our study covered a small area to demonstrate the importance of local variations in high RAC predictors. Obtaining a large number of measurements in a short period of time allowed us to reduce the influence of diurnal and other cycles characteristic of RAC in soil gas and its exhalation to the surface, and also to reduce the influence of cycles associated with diurnal meteorological and geodynamic cycles.

2. Materials and Methods

2.1. Study Area

The study area is located in the northern part of the Kuznetsk tectonic depression of the Hercynian folded-nappe structure (Figure 1).

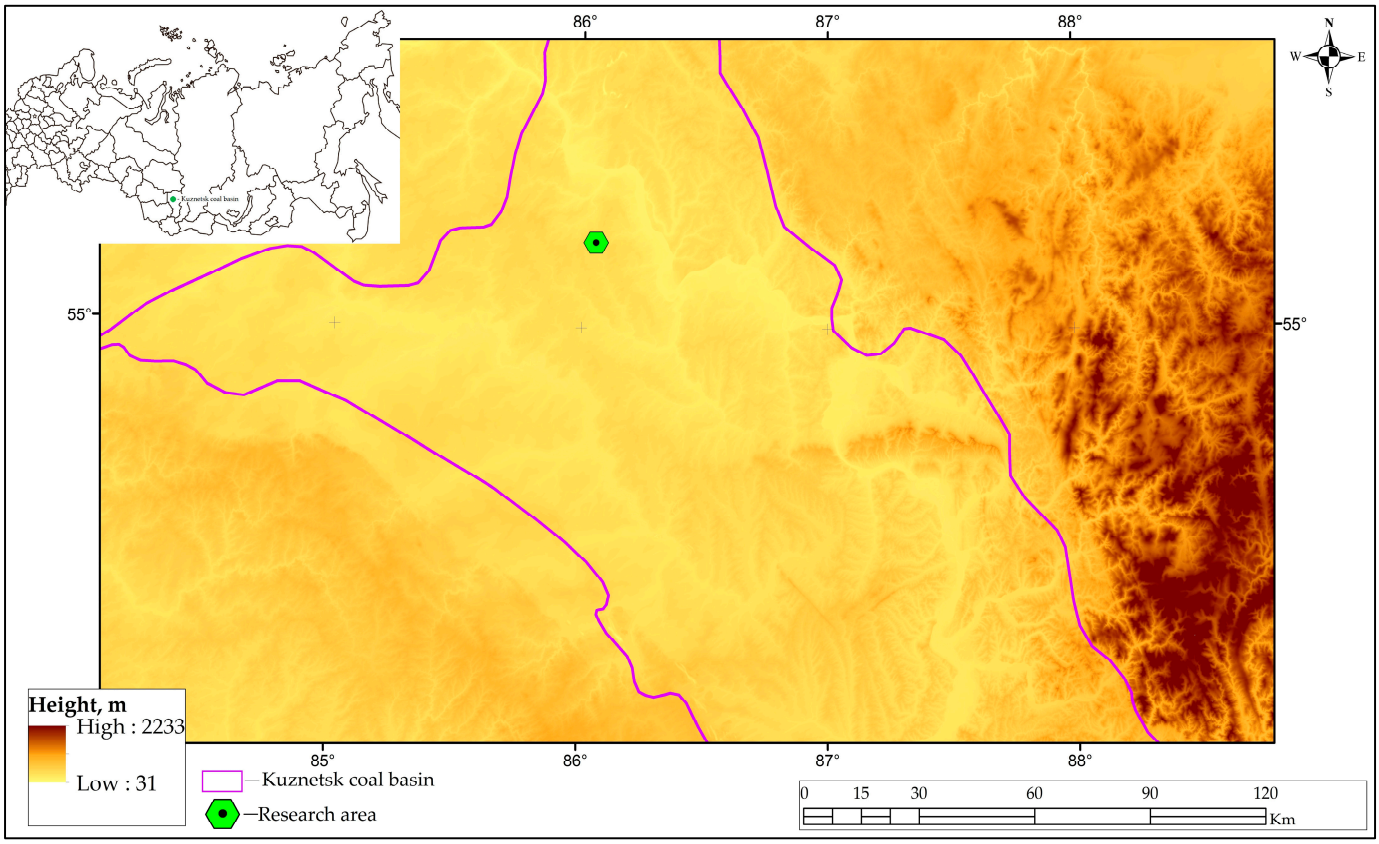

Figure 1. Map of the locations of sites for studying in Kuznetsk coal basin.

In geomorphological terms, the area is located on a polygenetic basement loess, prolluvial, lake-alluvial plain. Most of it is located on the left bank of the Tom River within the Kuznetsk Basin. It is composed of wide, flat, and gently sloping watersheds with elevation changes from 260 to 320 m. In the basement of the plain formed on the Cretaceous–Paleogene alignment surface, there are Paleozoic rocks (Permian and Jurassic coal-bearing sediment cycles) (Figure 2).

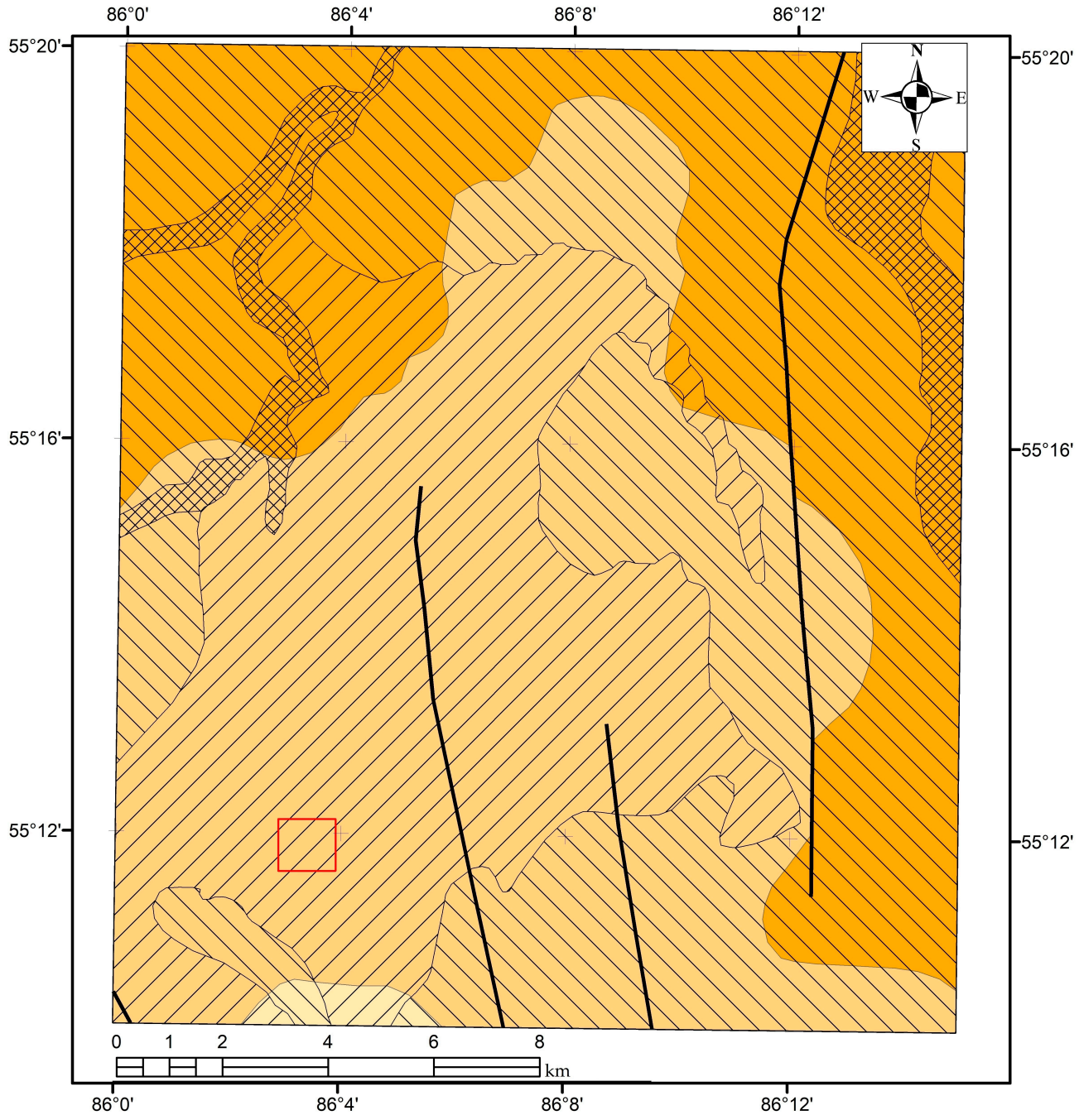

Figure 2. General geological map of the study area (compiled based on Lavrenov P.F. et al.) [46,47].

The structure of the loose cover includes loessoids of the Bachatskaya and Elovskaya formations with a total thickness of up to 50 m. The cover deposits of the study area are attributed to the Elovskaya formation of the upper link of the Neopleistocene of the Quaternary period. This formation covers the watersheds and floodplain terraces of Kuzbass in a mantle-like manner. Throughout the entire depression, deposits of this age cover the loessoids of the Bachatskaya formation, alluvial deposits of the terraces, or are located directly on the bedrock, as is observed in the studied area. In general, the formation corresponds to loess-like loams in terms of granulometric composition, among which medium and heavy varieties are found, and light varieties are less common [47].

In the composition of loams, the light fraction predominates (98–99%) and consists of quartz, feldspars, mica, and rock fragments [48]. The heavy fraction is dominated by epidote, amphiboles, and magnetite, and contains zircon, garnet, sphene, rutile, anatase, tourmaline, and apatite. The clay fraction consists of hydromicas, quartz, kaolinite, montmorillonite, calcite, and hematite. The thickness of the formation varies from 1 to 20 m. The formation of the lessoids was favored by the relatively calm tectonic environment and climatic conditions (there was a dry, cold climate) of the late Neopleistocene.

The relief surface is complicated by suffusion forms that developed on the loams of this formation in the Holocene. The cover deposits lie directly on the deposits of the upper part of the Krasnoyarsk formation (P_2ks_2), attributed to the middle section of the Permian system. The depth of this formation is approximately 15–20 m within the study area. It is represented by the interbedding of sandstones, siltstones, mudstones, and rarely encountered, intraformational conglomerates. The role of sandstones and conglomerates in the lower part of the formation increases, and of siltstones and mudstones it increases in the upper part. This subdivision is distinguished within the North Kuzbass facies zone, which is usually not characterized by the accumulation of organic matter in comparison with the approximately coeval Kazankovo–Markinskaya and Uskatskaya formations of Kuzbass. Various effusive rocks predominate among the fragments. The rocks are folded into a synclinal structure with very gentle wings. On both sides of the study site, there are supposed fault lines with a small uplift amplitude of up to 0.4 km and a fault displacement dip angle of 10 degrees to the east. The lines of these fault planes are located relatively far from the study area (from 1000 to 1500 m). No other disturbances were found during geological exploration in this area, but smaller disturbances, including those of Neogene-Quaternary age, are possible. Thus, for our territory, the most probable factors for radon emission are the physical properties of the soils of the cover deposits (loess-like loams, loams, and clays) and radioactivity (^{226}Ra content).

2.2. Radon Volumetric Activity in Soil Air

A total of 20 boreholes was drilled, and they were 1.5 m deep and 0.08 m in diameter, located in an orthogonal network, at a distance of about 130 m from each other (Figure 3).

A soil drill 2 m long and 0.08 m in diameter was used for drilling. After drilling, the boreholes were hermetically sealed with polyethylene film from the atmospheric air for at least 24 h. Then, control sampling of soil gas was carried out; in the event of crumbling of the walls or depressurization of the boreholes for any reason, these actions were repeated. After the final preparation of the boreholes for the study, they were left in a hermetically sealed state for 4–7 days before the start of measurements. Isolation was necessary to establish equilibrium between radon in the soil pore and the borehole.

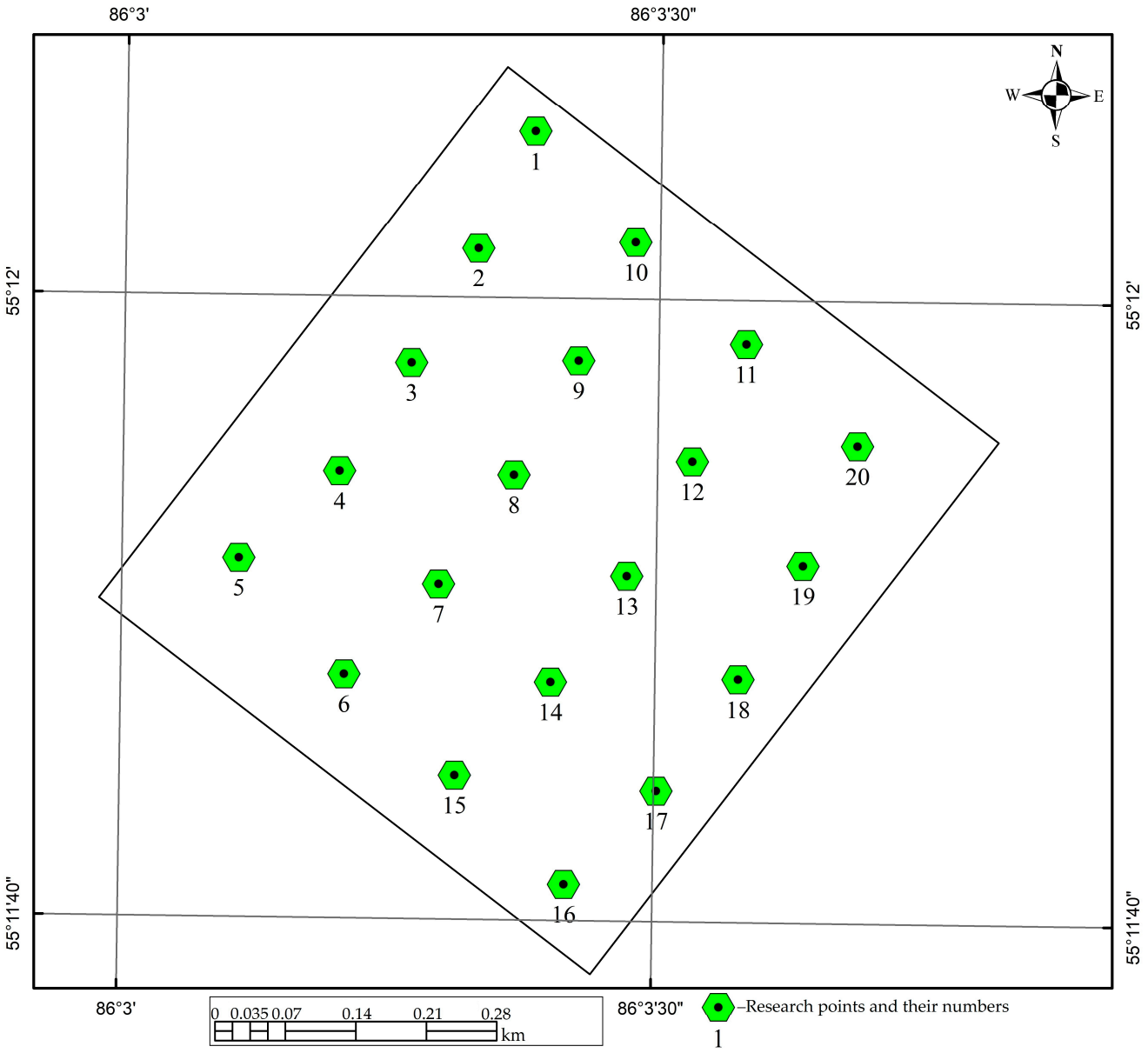

Figure 3. Scheme of measurements in the research area.

Radon was measured in two ways. The first measurement of RAC in the soil gas was carried out similarly to the study by [44]. Sampling was performed using a mobile air sampler AB-07 (NTM-Zashchita, Moscow, Russia). To obtain real values of RAC in the borehole, a closed-loop system was created between the borehole, air blower and the storage flask. The air sampler circulated air through this system for 5 min, thereby averaging the RAC in all parts of the system. In further analyses, a 50 mL storage flask was used. All elements of this system were isolated to prevent air leakage and, accordingly, radon loss from the borehole. The sampling itself was carried out from the bottom of the borehole using flexible hoses with a diameter of 2 mm, rigidly fixed to a plastic pipe. Sampling was carried out from the bottom of the borehole due to the high weight of radon. After each sample collection, the entire system was ventilated with atmospheric air for 5 min. The measurement of RAC was carried out on the Alfarad+ radiometer (Moscow, NTM "Zashchita", Russia). The basic principle of measurement was to estimate the concentration of ^{222}Rn in the radiometric chamber by its daughter product ^{218}Po, with a half-life of 3.05 min. The manufacturer's declared error of the device is no more than

±30%. For measurements, we tightly connected the storage flask and the internal detector chamber of the Alfarad+ and ventilated it with a blower built into the device in a closed system for 5 min to mix and average the values. The RAC was measured for 20 min in the "soil radon" mode. After each measurement, the Alfarad+ chamber was ventilated with atmospheric air for 5 min. Before measurements were taken, each collection flask was kept for 4 h to minimize the influence of shorter-lived radon isotopes (^{220}Rn) and their daughter decay products (DDP) on the result. We also repeated air sampling the next day in individual boreholes. The obtained values deviated from the previously obtained ones by 10–15% and did not exceed the declared measurement error of the device.

The second method of measuring the RAC in soil gas was carried out on sorption columns SC–13 using the Camera–01 complex (Moscow, Niton, Russia). The method is based on the passive sorption of radon in a room, borehole, or other object on activated carbon for 1–6 days and the subsequent measurement of the RAC on special sensors. The lower detection limit was 30 Bq/m^3. Sorption columns (SC–13) were filled with regenerated carbon and were weighed with an accuracy of 0.01 g by an OHAUS PX125D balance (OHAUS, Parsippany, NJ, USA). The column volume was 12.8 ± 0.6 cm^3, and the mass of the sorbent (activated carbon) was 5 ± 0.2 g. Before use, the carbon was regenerated and dehydrated in a drying chamber for 4 h at a temperature of 150–170 °C. Then the columns were lowered into each borehole to a depth of 1.4 m, which was necessary to eliminate the influence of vertical differences of the RAC in soil gas. The columns had a mesh on one side, through which radon freely entered, and after the study, this side was tightly closed with a lid. The exposure was 23–26 h, and then the sorption columns were tightly closed and sent to the laboratory. After that, the columns were re-weighed to account for the sorbed moisture from the borehole. This was necessary because moisture, as it accumulates, reduces the sorption potential of activated carbon for radon. When measuring radon on the Camera–01 equipment, the RAC was estimated based on the activity of its daughter decay products, ^{214}Pb and ^{214}Bi. The equilibrium with the parent element required for measurement was achieved by 4-h of holding before the study. This method also takes into account the weakening of the sorption properties of carbon when moisture accumulates. This exposure also minimized the influence of short-lived radon isotopes and their DDP on the analysis results.

RAC (C_{Rn}) was calculated using Equation (1) [49]:

$$C_{Rn} = \frac{A \times \exp(\lambda \times t)}{V} \quad (1)$$

where:

A is the total radon activity (Bq) in carbon at the end of sampling, Bq;
t is time (h) between the end of sampling and the start of measuring radon activity in carbon,
λ is the radon decay constant (0.00755 1/h),
V is the volumetric equivalent of SC–13 (m^3), determined by Equation (2) [49]:

$$V = 10^{-3} \times \exp\{1.58 + 0.307 \times \ln(t_{exp}) - 0.923 \times \sqrt{\Delta M} - 2.04 \times \sqrt{\Delta M} \times \exp(-0.0438 \times t_{exp})\} \quad (2)$$

where:

t_{exp} is the SC–13 sorption column passive sampling time (h),
and ΔM is the difference in mass (g) of SC–13 before and after exposure.

2.3. Measurement of Radon Flux Density (RFD)

The sampling and RFD calculation methods correspond to those used previously in our works [44,45]. Around each borehole, 5 research points were located, oriented in the

form of a square with a point in the center. At each point, there were 3 sorption columns, in total at each research point—15 sorption columns, and throughout the entire field of the RFD study—300. The RFD was estimated by the sorption method using the radon monitoring complex Camera–01 (NTC-NITON, Moscow, Russia). The principle of the method is passive sampling of radon as a result of its exhalation from the soil surface using accumulation chambers. An accumulation chamber (NK–32) was installed on the soil surface for 1–10 h (optimal is 5–6 h), which was a plastic container with a nylon mesh on the bottom and an opening in the upper part. The mesh ensured that radon exhalations from the soil entered the chamber, where it was sorbed on the surface of the coal. The upper opening was used to load activated carbon from the columns (SC–13) and then unload it after exposure. When the sensors were exposed, the upper opening was closed with an additional (protective) sorption column with activated carbon so that radon from the atmosphere did not penetrate into this chamber, but it remained open for air migration. The RFD was estimated using the Camera–01 device based on the gamma and beta radiation of short-lived DDP of ^{222}Rn decay—^{214}Pb and ^{214}Bi—which are in a state of radioactive equilibrium with radon. The coal that was previously loaded from the accumulation chamber (NK–32) into the sorption column was kept for 4 h to establish equilibrium between radon and its DDP and to minimize the effect of ^{220}Rn and its DDP on the activity of the coal. After that, it was loaded into the BDB–13 detection unit. Measurements on the device were carried out for 30 min. The error declared by the manufacturer of this method does not exceed 30%. The RFD measurement range was from 3 to 100,000 mBq m^{-2} s^{-1}. The air temperature should be between −5 and 40 °C. Relative humidity should not exceed 95% at an air temperature of 30 °C.

The RFD calculation was performed using Equation (3) [49]:

$$\sigma_{Rn} = \frac{\lambda \times A}{f \times S \times \{1 - \exp(-\lambda \times t_{exp})\}}, \quad (3)$$

where:

A is the radon activity (Bq) in the coal of the working layer NK–32 at the end of passive sampling,
λ is the radon decay constant (1/s),
t_{exp} is the duration (s) of coal sampling in chamber NK–32,
S is the working surface area NK–32, (m^2),
f is the correction factor taking into account the influence of NK–32 on the test object, rel. units.

Overall, the method allows for the assessment of radon exhalation from the soil, which provides information on soil permeability for radon. Repeated measurements at the same points were carried out in 15% of cases, and the results did not exceed the manufacturer's error of 30%, and in most cases, the error was less.

2.4. Measuring the Physical Properties of the Soil

Sampling was carried out from a depth of 1.5 m in sterile plastic containers with tightly closing lids.

We assessed the following physical properties of the soil:

- moisture,
- soil density,
- porosity, and
- void ratio (porosity coefficient).

The assessment method described in GOST 5180–2015 [50] and our other work was used with minor changes. Natural humidity was assessed by sequentially weighing the sample during drying at a temperature of 105 ± 2 °C. In this case, the assessment was made using Equation (4) [50]:

$$W = 100 \times \frac{m_1 - m_0}{m_0 - m} \quad (4)$$

where:

W is the soil moisture content (%),
m_1 is the mass (g) of wet soil with a weighing bottle,
m_0 is the mass (g) of dried soil with a weighing bottle,
and m is the mass (g) of an empty weighing bottle.

The natural density of the soil was measured by the standard procedure of weighing a paraffin-coated sample in water. In this case, the assessment was carried out according to Equation (5) [50]:

$$P = \frac{m \times p_p \times p_w}{p_p \times (m_1 - m_2) - p_w \times (m_1 - m)} \quad (5)$$

where:

m is the mass (g) of the soil sample before paraffin-coating,
m_1 is the mass (g) of the paraffin-coated sample,
m_2 is the result of weighing the sample in water—the difference between the mass of the paraffin-coated sample and the water displaced by it (g),
p_p is the density of the paraffin, taken to be 0.900 g/cm^3;
and p_w is the density of water at the test temperature, g/cm^3.

Soil porosity based on the density of soil particles and the skeleton (dry) of the soil was calculated using Equation (6) [51]:

$$n = \frac{P_s - P_d}{P_s} \quad (6)$$

where:

P_s is the density of soil particles, g/cm^3,
and P_d is the density of dry soil (g/cm^3).

The porosity coefficient demonstrates the ratio of the pore volume to the solid phase of the soil and was calculated using Equation (7) [51]:

$$e = \frac{P_s - P_d}{P_d} \quad (7)$$

where:

P_s is the density of soil particles (g/cm^3),
and P_d is the density of dry soil (g/cm^3).

2.5. Statistical Analysis

All data sets were tested for normality using the Kolmogorov–Smirnov and Shapiro–Wilk tests. Data comparisons between observation points were performed using the Kraskes–Wallis test ($p < 0.05$). Correlations were determined using the Spearman correlation coefficient ($p < 0.05$).

2.6. Spatial Analysis

The design of the interpolation models of various indicators (physical properties of soil, RFD, RAC in the soil gas, etc.) was performed using the inverse distance weighting (IDW) method in ArcGIS 10.8.1.

2.7. Meteorological Conditions During the Study

The design of the experiment implied taking samples in large quantities in a limited time interval. In this way, we tried to avoid the influence of meteorological factors that have a daily variation in influence [29].

During sampling by the air sampler, the temperature was 19–22 °C with an average value of 20.56 ± 0.23 °C, and the variation coefficient was 5%. The pressure was 981.3–981.5 hPa with an average value of 981.4 ± 0.03 hPa, and the variation coefficient had an extremely low value of 0.01%. The relative humidity was 47–60%, with an average value of 52.05 ± 0.85%, and the variation coefficient was 7.3%. The sampling was performed from 12:00 to 17:00 with a stable atmosphere and no precipitation.

The RFD was studied during the period of stable thermobaric conditions, from 10:00 to 19:00. The average exposure time of the sorption chambers was 6–7 h. The air temperature during the exposure period did not have significant differences. The average air temperature during the study period was 21.72 ± 0.31 °C and varied within a range of 20.28–23.30 °C with a variation coefficient of 6.42%. The atmospheric air pressure was 981.4–983.7 hPa with an average value of 982.5 ± 0.25 hPa and a variation coefficient of 0.12%. The relative humidity was 48.35–53.07% with an average of 51.39 ± 0.37% and a variation coefficient of 3.24%.

The meteorological conditions during the RAC measurement by the sorption method were also highly stable and had no significant pressure and temperature changes. The average exposure time of the sorption chambers was 25–27 h. The temperature was 19.83–20.03 with an average value of 19.91 ± 0.02, and the variation coefficient was 0.33%. The pressure was 974.1–974.5 hPa with an average value of 974.3 ± 0.03 hPa, and the variation coefficient was 0.01%. The relative humidity was 68.52–70.17%, with an average value of 69.42 ± 0.12%, and the variation coefficient was 0.78%. When studying soil radon in a similar way, but without taking into account the depth of the trap, the variation coefficients were also low—for temperature—0.15%, for pressure—0.01%, for humidity—0.44%. The variability of meteorological conditions during sampling was extremely low, as evidenced by the low variation coefficients for all measurements.

All meteorological data were collected from a meteorological station located near the study area. Additional verification of meteorological data was also carried out on site using a mobile weather station, Weather Station PCE-FWS 20N (PCE (Beijing) Technology Co., Ltd., Beijing, China). Due to the short distance and homogeneity of the landscape, we did not receive large differences between the data from the weather station and the mobile weather station.

3. Results

3.1. RAC in Soil Gas

The RAC in soil gas in 20 studied boreholes are presented in Table 1.

RAC vary widely, and repeated measurements by the active radon sampling method are not always within the error limits of the device (no more than 30%). Similar situations are noted at some points for the passive sorption method. But these deviations were noted in the case of the location of sorption columns (SC–13) or air intake hoses at some distance from the bottom, which was recognized when using an air sampler.

Table 1. RAC in soil gas obtained using active sampling with an air-sampler and passive sorption.

№	RAC in Soil Gas ± SE, Bq/m^3			
	Alpharad+		Camera–01	
	First Sampling	Second Sampling	1.4 m	Different Depth 1–1.4 m
1	20,877 ± 6263	28,346 ± 8503	33,500 ± 5000	28,200 ± 4200
2	12,975 ± 3892	10,601 ± 3180	26,100 ± 3900	10,300 ± 1500
3	29,975 ± 8992	30,786 ± 9235	38,200 ± 5700	35,100 ± 5300
4	26,062 ± 7818	26,214 ± 7864	28,300 ± 4200	27,400 ± 4100
5	26,303 ± 7890	29,171 ± 8751	34,900 ± 5200	27,800 ± 4200
6	42,173 ± 12,651	14,707 ± 4439	33,200 ± 5000	24,600 ± 3700
7	24,271 ± 7281	32,496 ± 9748	29,700 ± 4400	20,800 ± 3100
8	19,598 ± 5879	33,589 ± 10,076	22,700 ± 3400	23,000 ± 3400
9	31,804 ± 9541	18,834 ± 5650	37,500 ± 5600	24,400 ± 3600
10	27,446 ± 8233	25,971 ± 7791	33,100 ± 5000	24,800 ± 3700
11	28,366 ± 8509	–	33,500 ± 5000	26,900 ± 4000
12	24,182 ± 7254	–	48,500 ± 7300	40,200 ± 6000
13	27,771 ± 8331	–	47,300 ± 7100	33,600 ± 5000
14	22,653 ± 6795	–	23,700 ± 3500	23,200 ± 3500
15	20,596 ± 6178	–	22,500 ± 3400	18,300 ± 2700
16	28,481 ± 8544	–	33,800 ± 5000	24,900 ± 3700
17	28,800 ± 8640	–	39,400 ± 5900	29,000 ± 4300
18	22,234 ± 6670	–	27,400 ± 4100	26,800 ± 4000
19	23,595 ± 7078	–	29,100 ± 4400	30,100 ± 4500
20	21,698 ± 6509	–	30,200 ± 4500	28,700 ± 4300

Average values for the entire studied field obtained by both methods differ significantly (Table 2).

Table 2. Descriptive statistics for average RAC in soil gas values obtained by 2 methods.

Parameters	RAC in Soil Gas ± SE, Bq/m^3			
	Alpharad+		Camera–01	
	First Sampling	Second Sampling	1.4 m	Different Depth 1–1.4 m
Mean + St.er	25,493 ± 1311	25,072 ± 2462	32,630 ± 1600	26,405 ± 1396
Median	25,167	27,280	33,150	26,850
Min	12,975	10,601	22,500	10,300
Max	42,173	33,589	48,500	40,200
Coeff. Variance	22.99	31.06	21.93	23.64
25% Q	21,966	18,834	27,850	23,800
75% Q	28,424	30,786	36,200	28,850
St. Deviation	5862	7787	7156	6242

The Spearman correlation coefficient was calculated and high values were obtained for the pairs RAC 1.4 m/RAC 1–1.4 m (R = 0.70, $p < 0.01$) and the RAC first sample/RAC 1.4 m (R = 0.69, $p < 0.01$). At the same time, we obtained statistically significant differences between these pairs (K-W $p < 0.05$). For the remaining values, no correlation or differences were found. The highest RAC in soil gas values were obtained by the passive sorption method of the measurement in 1.4 m depth. This method also showed the lowest variation coefficient within the study field. Also, this method is not characterized by sporadic low

values, as in the others. Figure 4 shows the spatial results of RAC in soil gas obtained by different methods.

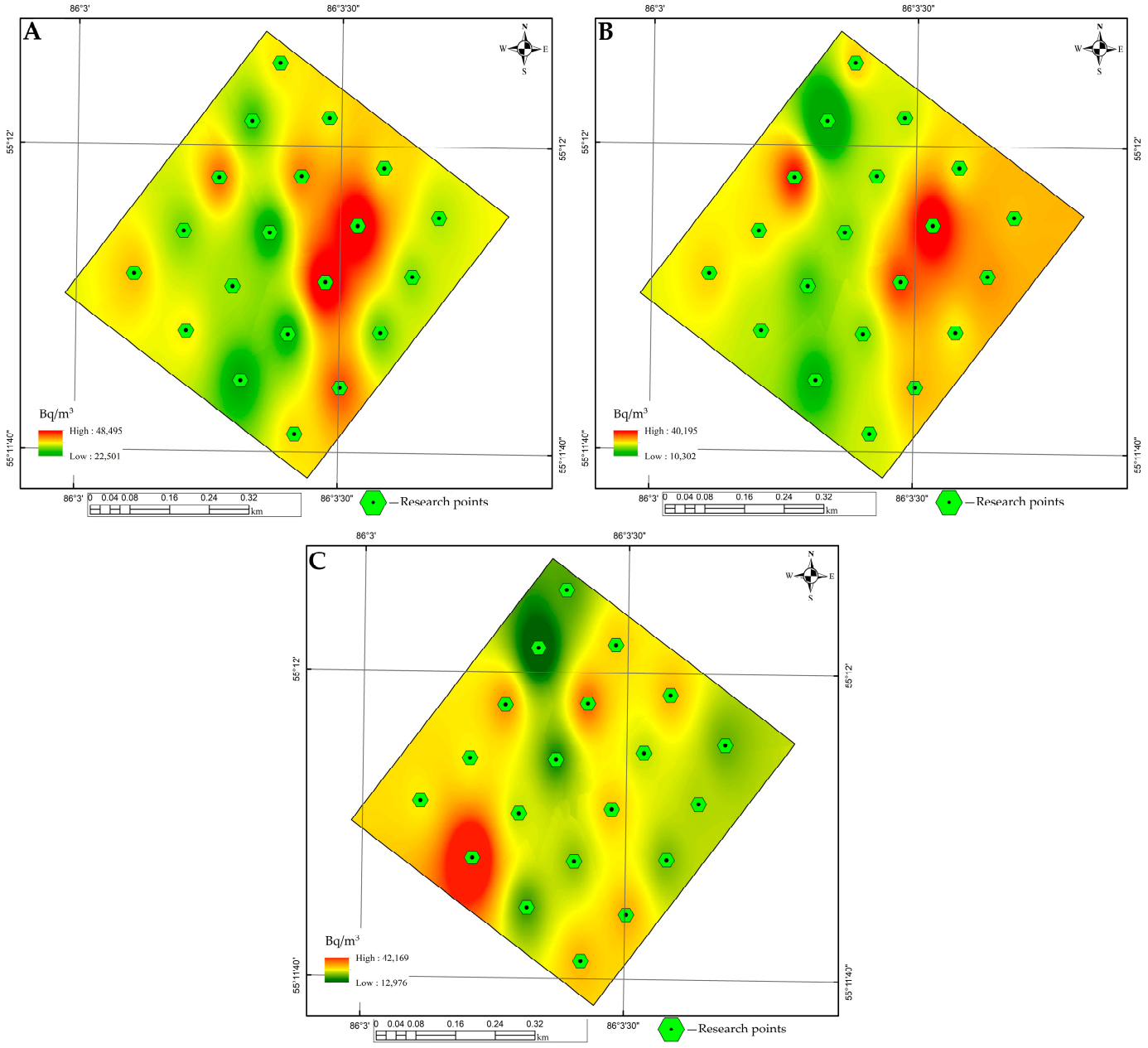

Figure 4. RAC in soil gas obtained by different methods. (**A**) sorption method (Camera–01) at a depth of 1.4 m; (**B**) sorption method (Camera–01) without taking depth into account (from 1 to 1.4 m); (**C**) indicator obtained using an air blower and a collection chamber (Alpharad+).

The data obtained by the sorption method in accordance with the depth formed a certain linear shape of the anomaly of high values. Some spatial similarity was observed between the data obtained by different methods. In the central part of the figure, a low RAC in soil gas value can be observed. A high spatial gradient between measurement points, mainly expressed from west to east, can be noted.

3.2. RFD

RFD for each point and for the entire studied field are presented in Table 3.

For all points, no significant deviation of RFD (more than 3 sigma) from the average value was observed. The minimum values were within the detection level of the device,

and the maximum did not exceed 100 mBq m^{-2} s^{-1}. The variation coefficients differed at each study point. For the entire study area, a fairly low variation coefficient (16.8%) can be concluded, and the variation within each point is from 18 to 46.2%. According to the regulatory documentation adopted in the Russian Federation—NRB99/2009 [52], this RFD field is classified as a safe territory, since the lower boundary corresponds to a value of 80 mBq m^{-2} s^{-1}. In our study, single measurements exceeded this value.

Table 3. RFD for the studied area.

No.	Radon Statistics, mBq m^{-2} s^{-1}							
	Mean + St.er	**Median**	**Min**	**Max**	**25% Q**	**75% Q**	**St. Deviation**	**Coeff. Variance**
1	33.6 ± 2.6	35	21	53	25	41	10.2	30.4
2	45 ± 5.1	45	22	99	27	54	19.6	43.6
3	28.3 ± 3.1	29	11	52	17	38	11.9	42.2
4	36.9 ± 2.9	36	19	55	28	48	11.3	30.6
5	41.1 ± 3	40	24	62	33	52	11.6	28.2
6	41.2 ± 3.9	40	20	65	28	58	15.0	36.3
7	35.2 ± 4	34	9	77	26	40	15.4	43.8
8	45.7 ± 3.5	47	18	73	39	54	13.5	29.5
9	23.9 ± 1.9	27	8	35	19	29	7.3	30.7
10	38.9 ± 2.8	37	19	61	35	45	10.5	26.9
11	33.8 ± 2.2	34	20	52	28	39	8.5	25.1
12	30.0 ± 3.6	31	9	50	19	45	13.9	46.2
13	36.0 ± 4.2	33	14	68	24	52	16.3	45.3
14	38.3 ± 2.1	38	27	58	33	42	7.9	20.7
15	48.3 ± 3.3	47	30	75	36	56	12.9	26.7
16	42.4 ± 2.8	40	26	62	35	50	10.7	25.2
17	42.1 ± 4.2	39	16	78	33	55	16.2	38.6
18	32.2 ± 3.4	30	10	58	24	40	13.3	41.3
19	32.5 ± 2.3	32	13	43	28	41	8.8	27.0
20	34.4 ± 1.6	35	22	46	31	38	6.2	18.0
Av	37 ± 1.4	36.5	23.9	48.3	33.1	41.6	6.2	16.8

Statistically significant differences (K-W test) were found between all observation points ($p < 0.01$). A matrix of differences was compiled for all points using the K-W criterion ($p < 0.05$) (Table 4).

Table 4. Matrix of differences of the RFD between observation points.

	1	2	3	4	5	6	7	8	9	10	11	12	13	14	15	16	17	18	19	20
1		-	-	-	-	-	-	+	+	-	-	-	-	-	+	+	-	-	-	-
2	-		+	-	-	-	-	-	+	-	-	+	-	-	-	-	-	-	+	-
3	-	+		-	+	+	-	+	-	+	-	-	-	+	+	+	+	-	-	-
4	-	-	-		-	-	-	-	+	-	-	-	-	-	+	-	-	-	-	-
5	-	-	+	-		-	-	-	+	-	-	-	-	-	-	-	-	-	-	-
6	-	-	+	-	-		-	-	+	-	-	-	-	-	-	-	-	-	-	-
7	-	-	-	-	-	-		+	+	-	-	-	-	-	+	-	-	-	-	-
8	+	-	+	-	-	-	+		+	-	+	+	-	-	-	-	-	+	+	+
9	+	+	-	+	+	+	+	+		+	+	-	+	+	+	+	+	-	+	+
10	-	-	+	-	-	-	-	-	+		-	-	-	-	-	-	-	-	-	-
11	-	-	-	-	-	-	-	+	+	-		-	-	-	+	+	-	-	-	-

Table 4. *Cont.*

	1	2	3	4	5	6	7	8	9	10	11	12	13	14	15	16	17	18	19	20
12	-	+	-	-	-	-	-	+	-	-	-		-	-	+	+	-	-	-	-
13	-	-	-	-	-	-	-	-	+	-	-	-		-	+	-	-	-	-	-
14	-	-	+	-	-	-	-	-	+	-	-	-	-		+	-	-	-	-	-
15	+	-	+	+	-	-	+	-	+	-	+	+	+	+		-	-	+	+	+
16	+	-	+	-	-	-	-	-	+	-	+	+	-	-	-		-	+	+	+
17	-	-	+	-	-	-	-	-	+	-	-	-	-	-	-	-		-	-	-
18	-	-	-	-	-	-	-	+	-	-	-	-	-	-	+	+	-		-	-
19	-	+	-	-	-	-	-	+	+	-	-	-	-	-	+	+	-	-		-
20	-	-	-	-	-	-	-	+	+	-	-	-	-	-	+	+	-	-	-	

-—there are no differences; +—there are differences.

High values are noted for point 9 (17/20 cases), 15 (11/20), 3, 8 (9/20), and 16 (8/20). For most of the study points, statistically significant differences were found with only a small number of other points.

Figure 5 shows the spatial characteristics of the RFD.

Spatially, the territory can be divided into two areas (southwest and northeast) with relatively high and low RFD values, respectively. There are also points with high RFD gradients relative to their neighbors.

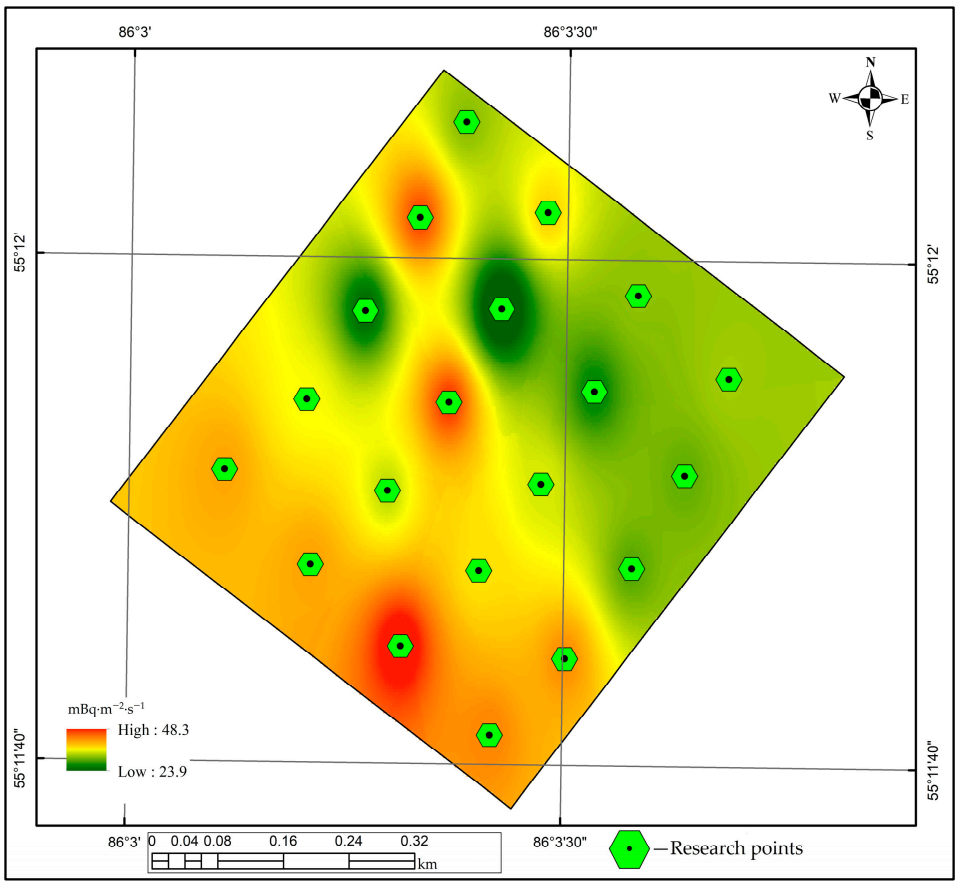

Figure 5. RFD.

3.3. Physical Properties of Soil

Physical properties of soil in the study area are presented in Table 5.

Table 5. Physical properties of soil in the study area.

1*	Mean + St.er	Median	Min	Max	25% Q	75% Q	St. Deviation	Coeff. Variance
P, g/cm^3	1.96 ± 0.01	1.95	1.86	2.06	1.92	1.99	0.06	2.82
W, %	26.4 ± 0.7	25.6	22.3	34.4	24.4	28.1	3	11.5
e, %	75 ± 2	76	64	94	69	78	7	9.50
n, %	43 ± 1	43	39	49	41	44	2	5.31

1*—Physical properties of soils: P—soil density, W—moisture, e—porosity coefficient, n—porosity.

The study area was characterized by loams of a fairly porous structure and high density of natural composition, while the humidity and porosity coefficient have a relatively small variation coefficient. The conditions for the emanation and migration of soil radon were quite uniform. However, these parameters can influence spatial differences of the RAC in soil gas. The soil conditions for the emanation and migration of radon were quite homogeneous.

The spatial features of the physical properties of the soil are presented in Figure 6.

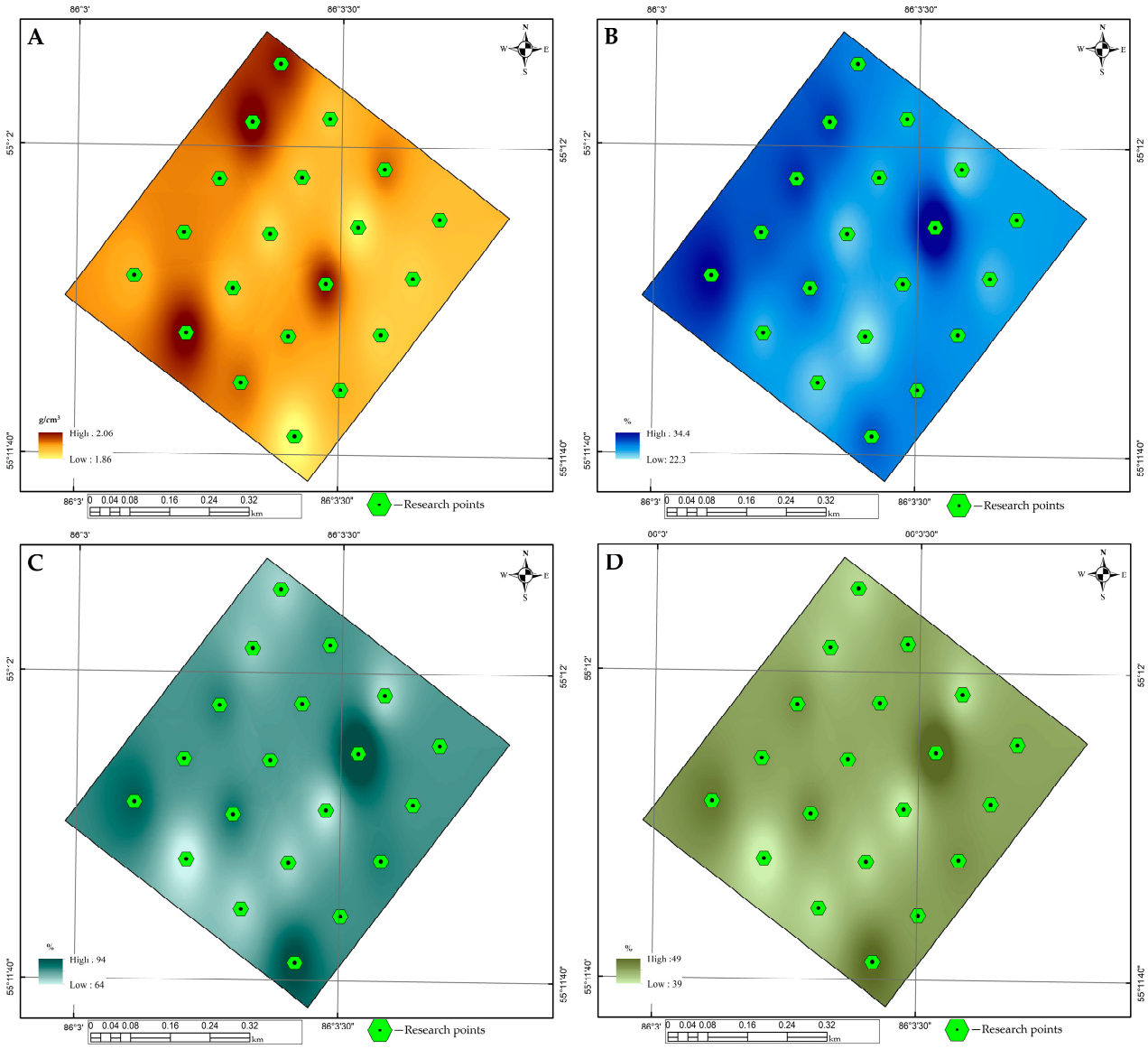

Figure 6. Physical properties of the soil. (**A**) soil density; (**B**) moisture; (**C**) porosity coefficient; (**D**) porosity.

The physical properties of the soil in the study area did not demonstrate a pronounced spatial structure with high and low values, i.e., there is most likely missing clustering in the data. The point form of small anomalies along the gradient of a relatively homogeneous field is characteristic. No spatially oriented features were noted within the study area. Meanwhile, some similarity is noted between the maps of soil moisture and porosity, which indicate the presence of pores filled with moisture. These point anomalies were also noted visually during field work, with the presence of higher visible moisture and even, in some cases, the accumulation of groundwater immediately after drilling.

3.4. Relationships Between RAC in Soil Gas, RFD, and Meteorological Indicators

The correlation matrix of the relationships between radiation hazard indicators (RFD and RAC in soil gas) and the physical properties of the soil and meteorological conditions is presented in Table 6.

Table 6. Correlation matrix.

Parameters		RFD	RAC (Alpharad+)	RAC–Different Depth 1–1.4 m (Camera–01)	RAC–1.4 m (Camera–01)
Radiologic parameters	RFD	–	No	–0.54 **	No
Physical properties of soil	P, g/cm^3	No	No	No	No
	W, %	No	No	No	0.44 *
	e, %	No	No	No	No
	n, %	No	No	No	No
Meteorological conditions	T, °C	–	No	–	–
	P, hPa	–	No	–	–
	H, %	–	No	–	–
	T, °C av. 1 h	–	No	–	–
	T, °C av. 2 h	–	No	–	–
	T, °C av. 3 h	–	No	–	–
	T, °C av. 4 h	–	No	–	–
	T, °C av. 5 h	–	No	–	–
	T, °C av. 6 h	–	No	–	–
	T, °C av. 7 h	–	No	–	–
	T, °C av. 8 h	–	No	–	–
	T, °C av. 9 h	–	No	–	–
	T, °C av. 10 h	–	No	–	–
	Tav	No	–	No	No
	Pav	No	–	No	No
	Hav	No	–	No	No
	Tmin	No	–	–	–
	Pmin	No	–	–	–
	Hmin	No	–	–	–
	Tmax	No	–	–	–
	Pmax	No	–	–	–
	Hmax	No	–	–	–
	Trange	No	–	–	–
	Prange	No	–	–	–
	Hrange	No	–	–	–

* $p < 0.05$; ** $p < 0.01$.

A correlation between soil moisture and radon concentration obtained by the sorption method was found as well as a negative correlation between RFD and VAR in soil air. No correlations were found for the remaining pairs of indicators.

4. Discussion

The entire territory of Kuzbass was previously classified as radon-hazardous [53]. This was mainly due to the geodynamic activity of the Altai Mountains and its northern mountain spurs. Our radon studies were conducted on a territory that is not associated with known fault structures within Kuzbass and the results obtained seem applicable to us in a real assessment of radon hazard.

The RFD in the study area can be considered safe, according to the existing standard (NRB-99/2009) [52]. The level that does not require any measures for migration of the penetration of geogenic radon into buildings is 80 $mBq \cdot m^{-2} \cdot s^{-1}$. In spatial terms, the southwestern part of the study area is an area of higher RFD, and the northeastern part of the area is an area of lower RFD. These areas are characterized by low spatial gradients between observation points, but also contain adjacent points with significantly higher gradients. It is noted that individual RFD points form statistically significant point anomalies with high gradients relative to adjacent points. These results are quite typical for RFD and are related to soil features at a more local level and the manifestation of spatial patterns at smaller scales. The absence of anomalies exceeding the average level by more than 3 sigma demonstrates that, in general, the area does not have areas with high radon exhalation to the surface, which could be associated with faults in the earth's crust, or high concentrations of ^{226}Ra. Thus, most likely, there is no deep radon migration, and its source is surface deposits. Previously, similar studies have shown that RFD is highly correlated with meteorological conditions (T, P, H) [31–34], including in Kuzbass [44,45]. The air temperature is usually able to influence the rate of radon exhalation to the daylight surface and reaches a maximum at the boundary of the environments (soil and atmosphere) [26,27,29]. Typically, this influence is expressed in daily and longer cycles of RFD changes on the day surface, and is in good agreement with similar temperature cycles [27,54–57]. In our study, this pattern was not found, but this does not exclude its presence. The most likely reason for this is the experimental design as RFD was measured over only a few days under highly stable meteorological conditions (variation coefficients 6.42% for T, 0.12% for P, and 3.24% for H). It should be noted separately that the coefficient of the variation of T, P, and H during the exposure of SC–13 sorption columns did not exceed 1%. Thus, at the 20 studied points, for each of which 15 measurements were made, the difference may be due to local variations in soil permeability and the content of ^{226}Ra in the surface soil horizons. Previously, the results of measuring the RFD, collected over longer periods and under different meteorological conditions, often had significant variability [44,45,58]. Also, the regularities of connections between meteorology and various types of radon migration in soils obtained earlier by Miklyaev P. and colleagues [41,59] confirm our conclusions about the dominance of diffusion transfer in the studied territory. Convective transfer is characterized by a pronounced correlation with the meteorological situation. These conclusions were obtained by them in a similar geological situation.

The RFD in the study area does not correlate with the RAC in the soil gas since it reflects the exhalation of radon from the upper soil horizon and depends significantly on atmospheric conditions and soil permeability. The horizon of our soil measurements was apparently located more deeply than the area in which the connections with the RFD were manifested. For similar soils, we have already obtained such a pattern in Kuznetsk tectonic depression [44,45].

The RAC in the soil gas is quite high if we rely on the Swedish radon hazard criterion. An indicator of $\geq$10 kBq/m^3 is typical for a moderate radon-hazardous area [60]. According to the maps in Figure 4, all areas are classified as areas where moderate radon protection is required. But this may be a consequence of the greater depth of boreholes, since it is known that most criteria are given for depths of 0.8–1 m, which is less than our boreholes. Previous studies have shown an increase of the RAC in soil gas with depth ([61–65]). According to the previously proposed criteria of Eisenbud and Gesell [66], the territory is considered moderately radon hazardous from 10 to 40 kBq/m^3 [60], and the Swedish criteria from 10 to 50 kBq/m^3. In our work, only the sorption method identified such territories in the region of 5% of the total area. All other methods did not demonstrate significant territories even above 40 kBq/m^3. But it is worth understanding that for a true assessment of radon

hazard, it is necessary to understand the permeability of the geological environment for radon. In this case, permeability is capable of changing under the influence of changing stress–strain conditions of the geological environment [67–69]. Figure 4 shows a high spatial gradient between measurement points, mainly from west to east. Overall, the RAC in soil gas is high for an area where pre-Cenozoic faults have not been identified. Potential causes may be the lack of detail in the geological survey here, the presence of a Neogene–Quaternary fault traced by a submeridional river, or high ^{226}Ra concentrations. It is known that Neogene–Quaternary faults do not always have a significant effect on the radon field [70]. When using sorption sampling of RAC in soil gas, a slightly lower variation coefficient is noted at higher values (mean, median, etc.) in relation to the method using an air sampler. Repeated measurements using an air sampler led to results close to the primary ones in terms of average values, but at certain points, quite serious deviations were observed. We assume here the influence of the sampling process; with incomplete immersion of the SC–13 sorption columns, the indicators may be underestimated since radon accumulates at the bottom of the boreholes. Given the low coefficient of variation, reduced probability of radon sampling from different depths, potentially lower influence of meteorological conditions and short geodynamic cycles, the sorption method seems more acceptable for radon monitoring. It looks especially promising for shallow boreholes.

According to our data, there are no significant correlations between the meteorological parameters of the atmosphere (at a level of 2 m above the surface) and radon indicators (RFD and RAC in soil gas, measured in two ways). When measuring RAC in soil gas by the sorption method, the role of meteorological conditions is even lower than when actively sampling from boreholes with an air sampler. The sorption method as an integral one, allowing estimation of the average RAC for a longer period. In our studies, conducted in another territory of Kuzbass, there was also no connection between meteorological conditions and RAC in soil gas for deep boreholes, and it was manifested only at depths of 0.6 and with some time lag at depths of 1 m and for air temperature. The soils were very similar in granulometry and other properties [61].

Soil physical properties did not show large differences between sites, but the variation coefficient decreased in the order W < e < n < P. Porosity and other soil properties usually have a significant effect on radon migration [71–74]. Soil moisture has a high variability within the study area and is likely to have the greatest effect on RAC in soil gas and radon migration in the soil. Such variability at the local level can significantly and randomly affect the final result at other study scales. This should be considered when making forecasts of the radon hazard of the territory. At this depth, water is mainly represented by hygroscopic and surface-film water, and as it gets deeper, the amount of free water (capillary and gravitational) increases. Soil moisture can affect the RAC and migration of radon in soil gas [33,75–78]. Radon mobility increases due to a decrease in the ability of radon to be sorbed on the surface of wet soil particles. With increasing humidity, pores and other voids in soils are occupied by moisture, which reduces radon mobility, i.e., the rate of diffusion and advection. Less dense soils, which simultaneously have a good emanation coefficient, will have a fairly high RAC in the soil gas. The obtained humidity values are generally consistent with the data obtained for the cover deposits of the Kuznetsk Basin of similar granulometric composition (25 to 20%) [79], which allows us to use the obtained results in predicting the behavior of radon in similar conditions, mainly with respect to cover deposits. A high proportion of pores in the rock volume (porosity), combined with an unchanged humidity indicator, leads to improved radon migration. High RAC in soil gas can be due to high soil moisture, which leads to a decrease in radon sorption in the soil and, accordingly, its migration into the borehole void [26,80]. But we did not find any correlations or spatial features, due to the multitude of predictors affecting RAC in soil

gas. Meanwhile, some similarity of the maps of soil moisture and porosity was noted, which indicates the presence of pores filled with moisture. These point anomalies were also noted visually during field work, with the presence of higher visible moisture and, even, in some cases, of groundwater accumulation immediately after drilling. The presence of point anomalies is most likely associated with the existence of clay lenses, which are aquicludes and affect the saturation of overlying strata with moisture.

Our study has some limitations that we considered when interpreting the results. Mainly, this is the lack of data on the content of ^{226}Ra, but the obtained RAC in the soil gas already allows us to consider it unsafe even without identifying the source of radon. For areas located on Paleozoic faults and the boundaries of mine workings, the RAC in soil gas is comparable to the obtained results. At the same time, the RFD differs quite strongly, and when compared with the areas of mine workings of Kuzbass, these differences are even greater. Considering that this territory was chosen as a background one based on primary tectonic features, surface deposits can be considered the source of radon until other sources are discovered. The study area is characterized by loamy soils, with slight differences in physical properties. As is known from earlier studies, for clays and loams, advection migration of radon will be difficult, including to the daylight surface, which is consistent with our low RFD values [81,82]. At the same time, these dispersion soils have a high emanation coefficient, i.e., the release of radon after its decay from ^{226}Ra [77].

We do not have our own data of this kind, but a number of works suggest a 40–60% emanation coefficient for these types of soils. It is also known that the predominant method of radon migration for them will be diffusion; it is usually limited to a length of 0.8 m. All these features indicate a high concentration of ^{226}Ra in the soil. The study of cover deposits in Kuzbass must be continued in connection with this circumstance.

Assuming that Kuzbass is characterized by predominantly diffusion transfer of radon, we do not exclude the existence of advective transfer of radon from deeper horizons, since some faults are currently active. Therefore, we intend to further study the composition and ratios of soil gases (CO_2, H_2, CH_4), which can be indicators of deeper migration of radon in the composition of "geogas" [16,83]. Simultaneous analysis of carbon and oxygen isotopes is also planned, which can help determine the depth and source of these gases in the geological environment [84,85]. To determine the areas of constant radon removal, we propose to study the ratios of lead ^{210}Pb and ^{226}Ra in soils, which, as expected, will disrupt their secular equilibrium in the gas phase (radon) of exhalation from the soil [86].

5. Conclusions

We have studied RAC in the soil gas in the territory outside the known fault structures within the Kuznetsk coal basin, and obtained important results that can be used in the real assessment of the radon hazard of the entire basin. The obtained RAC in soil gas is quite high, while its exhalation to the daylight surface is difficult, as evidenced by the low RFD. Since the dominant type of cover deposits in Kuznetsk coal basin, as in our study, are loams and clays, which are characterized by potentially high emanation coefficients, we can talk about the content of ^{226}Ra in cover soils as the most significant source of radon and a factor in the radon hazard of most territories. The diffusion migration of radon will be dominant in these conditions. Thus, the obtained results allow us to formulate the correct methodology for studying the radon hazard of the Kuznetsk coal basin.

Author Contributions: Conceptualization, T.L. and A.L.; methodology, T.L.; software, T.L.; validation, K.L., T.L., E.B. and A.L.; formal analysis, T.L. and A.L.; investigation, K.L., T.L., E.B. and A.L.; resources, T.L. and A.L.; data curation, T.L.; writing—original draft preparation, T.L. and A.L.; writing—review and editing, K.L., T.L. and A.L.; visualization, T.L.; supervision, T.L.; project administration, A.L.; funding acquisition, A.L. All authors have read and agreed to the published version of the manuscript.

Funding: This research was funded by the Russian Science Foundation (RSF), under research project № 23-27-00320, https://rscf.ru/en/project/23-27-00320/ (accessed on 30 September 2024).

Data Availability Statement: The data presented in this study are available in the article.

Conflicts of Interest: The authors declare no conflicts of interest.

References

1. Toader, V.-E.; Mihai, A.; Moldovan, I.-A.; Ionescu, C.; Marmureanu, A.; Lingvay, I. Implementation of a Radon Monitoring Network in a Seismic Area. *Atmosphere* **2021**, *12*, 1041. [CrossRef]
2. Riudavets, M.; Garcia de Herreros, M.; Besse, B.; Mezquita, L. Radon and Lung Cancer: Current Trends and Future Perspectives. *Cancers* **2022**, *14*, 3142. [CrossRef]
3. Malinovsky, G.; Yarmoshenko, I.; Zhukovsky, M. Radon, Smoking and HPV as Lung Cancer Risk Factors in Ecological Studies. *Int. J. Radiat. Biol.* **2018**, *94*, 62–69. [CrossRef] [PubMed]
4. Chen, J.; Ford, K.L. A Study on the Correlation between Soil Radon Potential and Average Indoor Radon Potential in Canadian Cities. *J. Environ. Radioact.* **2017**, *166*, 152–156. [CrossRef] [PubMed]
5. Borgoni, R.; Tritto, V.; Bigliotto, C.; De Bartolo, D. A Geostatistical Approach to Assess the Spatial Association between Indoor Radon Concentration, Geological Features and Building Characteristics: The Case of Lombardy, Northern Italy. *Int. J. Environ. Res. Public Health* **2011**, *8*, 1420–1440. [CrossRef]
6. Kemski, J.; Klingel, R.; Siehl, A.; Valdivia-Manchego, M. From Radon Hazard to Risk Prediction-Based on Geological Maps, Soil Gas and Indoor Measurements in Germany. *Environ. Geol.* **2009**, *56*, 1269–1279. [CrossRef]
7. Briones, C.; Jubera, J.; Alonso, H.; Olaiz, J.; Santana, J.T.; Rodríguez-Brito, N.; Arriola-Velásquez, A.C.; Miquel, N.; Tejera, A.; Martel, P.; et al. Multiparametric Analysis for the Determination of Radon Potential Areas in Buildings on Different Soils of Volcanic Origin. *Sci. Total Environ.* **2023**, *885*, 163761. [CrossRef] [PubMed]
8. Di Carlo, C.; Maiorana, A.; Ampollini, M.; Antignani, S.; Caprio, M.; Carpentieri, C.; Bochicchio, F. Models of Radon Exhalation from Building Structures: General and Case-Specific Solutions. *Sci. Total Environ.* **2023**, *885*, 163800. [CrossRef]
9. Yarmoshenko, I.V.; Malinovsky, G.P.; Zhukovsky, M.V.; Izgagin, V.S.; Onishchenko, A.D.; Vasilyev, A.V. Ra-226 in Building Materials as a Source of Indoor Radon in High-Rise Residential Buildings in Russian Cities. *Sci. Total Environ.* **2024**, *935*, 173492. [CrossRef] [PubMed]
10. Chen, J.; Rahman, N.M.; Atiya, I.A. Radon Exhalation from Building Materials for Decorative Use. *J. Environ. Radioact.* **2010**, *101*, 317–322. [CrossRef] [PubMed]
11. Santamarta, J.; Hernández-Gutiérrez, L.E.; Rodríguez-Martín, J.; Hernández, A.; Gutierrez-Villanueva, J.L.; Cruz-Pérez, N. Radon Measurements in Public Buildings in El Hierro, Canary Islands (Spain). *Air Qual. Atmos. Health* **2021**, *14*, 895–902. [CrossRef]
12. Yarmoshenko, I.; Malinovsky, G.; Vasilyev, A.; Onishchenko, A. Model of Radon Entry and Accumulation in Multi-Flat Energy-Efficient Buildings. *J. Environ. Chem. Eng.* **2021**, *9*, 105444. [CrossRef]
13. Dyck, W.; Jonasson, I.R. Chapter 11 Radon. In *Handbook of Exploration Geochemistry*; Hale, M., Ed.; Geochemical Remote Sensing of the Sub-Surface; Elsevier Science B.V.: Amsterdam, The Netherlands, 2000; Volume 7, pp. 353–394.
14. Etiope, G.; Lombardi, S. Laboratory Simulation of Geogas Microbubble Flow. *Environ. Geol.* **1996**, *27*, 226–232. [CrossRef]
15. Etiope, G.; Martinelli, G. Migration of Carrier and Trace Gases in the Geosphere: An Overview. *Phys. Earth Planet. Inter.* **2002**, *129*, 185–204. [CrossRef]
16. Chen, X.; Liu, Y.; Jiang, Y.; Feng, S. Radon Transport Carried by Geogas: Prediction Model. *Environ. Sci. Pollut. Res.* **2023**, *30*, 86656–86675. [CrossRef]
17. Voltattorni, N.; Sciarra, A.; Quattrocchi, F. The Application of Soil Gas Technique to Geothermal Exploration: Study of "Hidden" Potential Geothermal Systems. In Proceedings of the World Geothermal Congress, Bali, Indonesia, 25 April 2010.
18. Voltattorni, N.; Gasparini, A.; Galli, G. The Analysis of 222Rn and 220Rn Natural Radioactivity for Local Hazard Estimation: The Case Study of Cerveteri (Central Italy). *Int. J. Environ. Res. Public Health* **2023**, *20*, 6420. [CrossRef] [PubMed]
19. Seminsky, K.Z.; Bobrov, A.A. Radon Activity of Faults (Western Baikal and Southern Angara Areas). *Russ. Geol. Geophys.* **2009**, *50*, 682–692. [CrossRef]

20. Seminskii, K.; Bobrov, A.A.; Sodnomsambuu, D. Relationship between Radon and the Tectonic Activity of Faults in Central Mongolia. *Dokl. Earth Sci.* **2019**, *487*, 890–893. [CrossRef]
21. Utkin, V.I.; Yurkov, A.K. Radon as a Tracer of Tectonic Movements. *Russ. Geol. Geophys.* **2010**, *51*, 220–227. [CrossRef]
22. Pereira, A.J.S.C.; Godinho, M.M.; Neves, L.J.P.F. On the Influence of Faulting on Small-Scale Soil-Gas Radon Variability: A Case Study in the Iberian Uranium Province. *J. Environ. Radioact.* **2010**, *101*, 875–882. [CrossRef] [PubMed]
23. Wang, N.; Yang, J.; Wang, H.; Jia, B.; Peng, A. Characteristics of Indoor and Soil Gas Radon, and Discussion on High Radon Potential in Urumqi, Xinjiang, NW China. *Atmosphere* **2023**, *14*, 1548. [CrossRef]
24. Sajwan, R.S.; Joshi, V.; Ahamad, T.; Kumar, N.; Parmar, P.; Jindal, M.K. Assessment of Radon Transportation and Uranium Content in the Tectonically Active Zone of Himalaya, India. *Sci. Total Environ.* **2024**, *926*, 171823. [CrossRef] [PubMed]
25. Voltattorni, N.; Gasparini, A.; Cinti, D.; Galli, G.; Procesi, M. Analyzing the 222Rn/220Rn Ratio in a Seismic Area: A Reliable Method to Understand the Development of Active Structural Discontinuities in Earthquake Surveillance and Sustainability. *Sustainability* **2024**, *16*, 10449. [CrossRef]
26. Benkovitz, A.; Zafrir, H.; Reuveni, Y. A Novel Assessment of the Surface Heat Flux Role in Radon (Rn-222) Gas Flow within Subsurface Geological Porous Media. *Remote Sens.* **2023**, *15*, 4094. [CrossRef]
27. Haquin, G.; Zafrir, H.; Ilzycer, D.; Weisbrod, N. Effect of Atmospheric Temperature on Underground Radon: A Laboratory Experiment. *J. Environ. Radioact.* **2022**, *253–254*, 106992. [CrossRef]
28. Zafrir, H.; Barbosa, S.; Levintal, E.; Weisbrod, N.; Ben Horin, Y.; Zalevsky, Z. The Impact of Atmospheric and Tectonic Constraints on Radon-222 and Carbon Dioxide Flow in Geological Porous Media—A Dozen-Year Research Summary. *Front. Earth Sci.* **2020**, *8*, 433. [CrossRef]
29. Benkovitz, A.; Zafrir, H.; Reuveni, Y. The Dynamics of Rn-222 Cyclic Flow within the Shallow Geological Subsurface Media as a Daily Temporal Variated Source for Exhalation into the Air. *Sci. Total Environ.* **2024**, *912*, 169244. [CrossRef] [PubMed]
30. Čeliković, I.; Pantelić, G.; Vukanac, I.; Nikolić, J.K.; Živanović, M.; Cinelli, G.; Gruber, V.; Baumann, S.; Ciotoli, G.; Poncela, L.S.Q.; et al. Overview of Radon Flux Characteristics, Measurements, Models and Its Potential Use for the Estimation of Radon Priority Areas. *Atmosphere* **2022**, *13*, 2005. [CrossRef]
31. Miklyaev, P.S.; Petrova, T.B.; Shchitov, D.V.; Sidyakin, P.A.; Murzabekov, M.A.; Tsebro, D.N.; Marennyy, A.M.; Nefedov, N.A.; Gavriliev, S.G. Radon Transport in Permeable Geological Environments. *Sci. Total Environ.* **2022**, *852*, 158382. [CrossRef]
32. Muhammad, A.; Danbatta, S.J.; Muhammad, I.Y.; Nasidi, I.I. Exploring Soil Radon (Rn) Concentrations and Their Connection to Geological and Meteorological Factors. *Environ. Sci. Pollut. Res.* **2024**, *31*, 565–578. [CrossRef] [PubMed]
33. Yang, J.; Busen, H.; Scherb, H.; Hürkamp, K.; Guo, Q.; Tschiersch, J. Modeling of Radon Exhalation from Soil Influenced by Environmental Parameters. *Sci. Total Environ.* **2019**, *656*, 1304–1311. [CrossRef] [PubMed]
34. Kamra, L. Seasonal Emanation of Radon at Ghuttu, Northwest Himalaya: Differentiation of Atmospheric Temperature and Pressure Influences. *Appl. Radiat. Isot.* **2015**, *105*, 170–175. [CrossRef]
35. Szabó, K.Z.; Jordan, G.; Horváth, Á.; Szabó, C. Mapping the Geogenic Radon Potential: Methodology and Spatial Analysis for Central Hungary. *J. Environ. Radioact.* **2014**, *129*, 107–120. [CrossRef] [PubMed]
36. Kropat, G.; Bochud, F.; Murith, C.; Palacios (Gruson), M.; Baechler, S. Modeling of Geogenic Radon in Switzerland Based on Ordered Logistic Regression. *J. Environ. Radioact.* **2017**, *166*, 376–381. [CrossRef]
37. Bossew, P.; Cinelli, G.; Ciotoli, G.; Crowley, Q.G.; De Cort, M.; Elío Medina, J.; Gruber, V.; Petermann, E.; Tollefsen, T. Development of a Geogenic Radon Hazard Index—Concept, History, Experiences. *Int. J. Environ. Res. Public Health* **2020**, *17*, 4134. [CrossRef] [PubMed]
38. Choi, Y.; Bae, M.S.; Oh, Y.; Lee, S. Predictive Geogenic Radon Potential (P-GRP): A Novel Approach for Comprehensive Hazard Assessment and Risk Modeling in Subsurface Environment. *Sci. Total Environ.* **2024**, *944*, 173721. [CrossRef]
39. Masoumi, I.; Maggio, S.; De Iaco, S.; Ghezelbash, R. Spatial Multi-Criteria Approaches for Estimating Geogenic Radon Hazard Index. *Sci. Total Environ.* **2024**, *956*, 176419. [CrossRef]
40. Petermann, E.; Bossew, P.; Kemski, J.; Gruber, V.; Suhr, N.; Hoffmann, B. Development of a High-Resolution Indoor Radon Map Using a New Machine Learning-Based Probabilistic Model and German Radon Survey Data. *Environ. Health Perspect.* **2024**, *132*, 97009. [CrossRef]
41. Gavriliev, S.; Petrova, T.; Miklyaev, P.; Karfidova, E. Predicting Radon Flux Density from Soil Surface Using Machine Learning and GIS Data. *Sci. Total Environ.* **2023**, *903*, 166348. [CrossRef] [PubMed]
42. Dicu, T.; Cucoş, A.; Botoş, M.; Burghele, B.; Florică, Ş.; Baciu, C.; Ştefan, B.; Bălc, R. Exploring Statistical and Machine Learning Techniques to Identify Factors Influencing Indoor Radon Concentration. *Sci. Total Environ.* **2023**, *905*, 167024. [CrossRef] [PubMed]
43. Benà, E.; Ciotoli, G.; Petermann, E.; Bossew, P.; Ruggiero, L.; Verdi, L.; Huber, P.; Mori, F.; Mazzoli, C.; Sassi, R. A New Perspective in Radon Risk Assessment: Mapping the Geological Hazard as a First Step to Define the Collective Radon Risk Exposure. *Sci. Total Environ.* **2024**, *912*, 169569. [CrossRef] [PubMed]
44. Leshukov, T.; Legoshchin, K.; Larionov, A. Radon Hazard of the Zhurinsky Fault for the Population in the Kuznetsk Coal Basin: Primary Results. *Sustainability* **2023**, *15*, 16774. [CrossRef]

45. Leshukov, T.; Legoshchin, K.; Larionov, A. A Case Study of the Radon Hazard at the Boundary of a Coal Minefield. *Appl. Sci.* **2023**, *13*, 13188. [CrossRef]
46. Lavrenov, P.F.; Snegko, B.A.; Shigrev, A.F.; Shelemeteva, A.V.; Filippova, N.V. *State Geological Map of the Russian Federation. Scale 1: 200,000*, 2nd ed.; Kuzbass Series. Sheet N-45-XV (Leninsk-Kuznetsky). Explanatory Letter; VSEGEI: Moscow, Russia, 2018.
47. Lavrenov, P.F.; Snegko, B.A.; Shigrev, A.F.; Dmitrieva, N.V.; Filippova, N.E.; Noskov, Y.S.; Zeifert, L.L. *State Geological Map of the Russian Federation. Scale 1: 200,000*, 2nd ed.; Kuzbass Series. Sheet N-45-IX (Krapivinsky). Explanatory Letter; VSEGEI: Moscow, Russia, 2015.
48. Ryabchikova, E.D. Pleistocene Loess-like Deposits of the Southwestern Part of the Kuznetsk Basin (Their Structure, Lithology and Conditions of Formation). Candidate's Thesis, TPU, Tomsk, Russia, 1971; 24p.
49. *Measuring Complex for Radon Monitoring "CAMERA-01". Passport*; Scientific and Technical Center "NITON": Moskow, Russia, 2003.
50. *GOST 5180-2015*; SOILS Laboratory Methods for Determining Physical Characteristics. Interstate Council for Standardization, Metrology and Certification (ISC). Standartinform: Moscow, Russia, 2016.
51. *GOST 25100-2011*; Soils. Classification. Standartinform: Moscow, Russia, 2018.
52. *NRB99/2009*; Radiation Safety Standards: Sanitary and Epidemiological Rules and Regulations. Federal Center for Hygiene and Epidemiology of Rospotrebnadzor: Moscow. Russia, 2009.
53. Maksimovskij, V.A.; Reshetov, V.V.; Harlamov, M.G. Radon Hazard Map of Russia 1995. Available online: https://www.researchgate.net/figure/radon-hazard-map-of-russia-for-1995-86_fig18_377548215 (accessed on 25 September 2024).
54. Lefebvre, R.; Lahmira, B.; Löbner, W. Atmospheric Control of Radon Emissions from a Waste Rock Dump. *Environ. Geotech.* **2019**, *6*, 381–392. [CrossRef]
55. Miklyaev, P.S.; Petrova, T.B.; Marennyy, A.M.; Shchitov, D.V.; Sidyakin, P.A.; Murzabekov, M.A.; Lopatin, M.N. High Seasonal Variations of the Radon Exhalation from Soil Surface in the Fault Zones (Baikal and North Caucasus Regions). *J. Environ. Radioact.* **2020**, *219*, 106271. [CrossRef] [PubMed]
56. Miklyaev, P.S.; Petrova, T.B.; Shchitov, D.V.; Sidyakin, P.A.; Murzabekov, M.A.; Marennyy, A.M.; Nefedov, N.A.; Sapozhnikov, Y.A. The Results of Long-Term Simultaneous Measurements of Radon Exhalation Rate, Radon Concentrations in Soil Gas and Groundwater in the Fault Zone. *Appl. Radiat. Isot.* **2021**, *167*, 109460. [CrossRef]
57. Yang, J.; Buchsteiner, M.; Salvamoser, J.; Irlinger, J.; Guo, Q.; Tschiersch, J. Radon Exhalation from Soil and Its Dependence from Environmental Parameters. *Radiat. Prot. Dosim.* **2017**, *177*, 21–25. [CrossRef] [PubMed]
58. Leshukov, T.; Larionov, A.; Legoshchin, K.; Lesin, Y.; Yakovleva, S. The Assessment of Radon Emissions as Results of the Soil Technogenic Disturbance. *Int. J. Environ. Res. Public Health* **2020**, *17*, 9268. [CrossRef] [PubMed]
59. Gavriliev, S.; Petrova, T.; Miklyaev, P. Factors Influencing Radon Transport in the Soils of Moscow. *Environ. Sci. Pollut. Res.* **2022**, *29*, 88606–88617. [CrossRef] [PubMed]
60. Lara, E.; Rocha, Z.; Palmieri, H.E.L.; Santos, T.O.; Rios, F.J.; Oliveira, A.H. Radon Concentration in Soil Gas and Its Correlations with Pedologies, Permeabilities and 226Ra Content in the Soil of the Metropolitan Region of Belo Horizonte—RMBH, Brazil. *Radiat. Phys. Chem.* **2015**, *116*, 317–320. [CrossRef]
61. Leshukov, T.; Legoshchin, K.; Avdeev, K.; Baranova, E.; Larionov, A. Depth Gradient and Radon Activity Concentration in Soil Gas in the Zone of a Potentially Active Fault. *Earth* **2024**, *5*, 1005–1022. [CrossRef]
62. Mao, Y.; Zhang, L.; Wang, H.; Guo, Q. The Temporal Variation of Radon Concentration at Different Depths of Soil: A Case Study in Beijing. *J. Environ. Radioact.* **2023**, *264*, 107200. [CrossRef] [PubMed]
63. Barnet, I.; Pacherová, P. Gamma Dose Rate and Soil Gas Radon Concentration Measured at Low Soil Thickness (Czech Republic). *Environ. Earth Sci.* **2016**, *75*, 620. [CrossRef]
64. Catalano, R.; Immé, G.; Mangano, G.; Morelli, D.; Aranzulla, M. Radon Transport: Laboratory and Model Study. *Radiat. Prot. Dosim.* **2015**, *164*, 575–581. [CrossRef] [PubMed]
65. Mitev, K.; Dutsov, C.; Georgiev, S.; Boshkova, T.; Pressyanov, D. Unperturbed, High Spatial Resolution Measurement of Radon-222 in Soil-Gas Depth Profile. *J. Environ. Radioact.* **2019**, *196*, 253–258. [CrossRef]
66. Eisenbud, M.; Gesell, T.F. *Environmental Radioactivity: From Natural, Industrial and Military Sources*; Elsevier Science: Amsterdam, The Netherlands, 1997; ISBN 978-0-12-235154-9.
67. Zaalishvili, V.B.; Melkov, D.A.; Martyushev, N.V.; Klyuev, R.V.; Kukartsev, V.V.; Konyukhov, V.Y.; Kononenko, R.V.; Gendon, A.L.; Oparina, T.A. Radon Emanation and Dynamic Processes in Highly Dispersive Media. *Geosciences* **2024**, *14*, 102. [CrossRef]
68. Kozlova, I.A.; Yurkov, A.K.; Biryulin, S.V. Variations in the volume activity of radon during technogenic and tectonic seismic events. *GIAB* **2022**, *5*, 119–130. [CrossRef]
69. Zaalishvili, V.; Melkov, D.; Revazov, M. Relationship of Radon Emanation with the Level of External Impact According to Large Landslides Monitoring in Mountain Areas. *Sustain. Dev. Mt. Territ.* **2021**, *13*, 564–575. [CrossRef]
70. Mair, J.; Petermann, E.; Lehné, R.; Henk, A. Can Neotectonic Faults Influence Soil Air Radon Levels in the Upper Rhine Graben? An Exploratory Machine Learning Assessment. *Sci. Total Environ.* **2024**, *956*, 177179. [CrossRef]

71. Li, P.; Sun, Q.; Geng, J.; Shi, Q.; Hu, J.; Tang, S. A Study on the Differences in Radon Exhalation of Different Lithologies at Various Depths and the Factors Influencing Its Distribution in Northern Shaanxi, China. *Sci. Total Environ.* **2022**, *849*, 157935. [CrossRef] [PubMed]
72. Zheng, X.; Sun, Q.; Jing, X.; Yang, D.; Jia, H. Evolution of Pore Structure and Radon Exhalation Characterization of Porous Media Grouting. *Sci. Total Environ.* **2023**, *865*, 161352. [CrossRef]
73. Markkanen, M.; Arvela, H. Radon Emanation from Soils. *Radiat. Prot. Dosim.* **1992**, *45*, 269–272. [CrossRef]
74. Dardac, M.; Elío, J.; Aghdam, M.M.; Banríon, M.; Crowley, Q. Application of Airborne Geophysical Survey Data in a Logistic Regression Model to Improve the Predictive Power of Geogenic Radon Maps. A Case Study in Castleisland, County Kerry, Ireland. *Sci. Total Environ.* **2023**, *894*, 164965. [CrossRef] [PubMed]
75. Benavente, D.; Pla, C. Effect of Pore Structure and Moisture Content on Gas Diffusion and Permeability in Porous Building Stones. *Mater. Struct.* **2018**, *51*, 21. [CrossRef]
76. Li, P.; Sun, Q.; Cong, L. Study on the Influence of Water Saturation on Radon Exhalation Rates of Rocks. *Sci. Total Environ.* **2024**, *946*, 174192. [CrossRef]
77. Benavente, D.; Valdés-Abellán, J.; Pla, C.; Sanz-Rubio, E. Estimation of Soil Gas Permeability for Assessing Radon Risk Using Rosetta Pedotransfer Function Based on Soil Texture and Water Content. *J. Environ. Radioact.* **2019**, *208–209*, 105992. [CrossRef] [PubMed]
78. Gil-Oncina, S.; Valdes-Abellan, J.; Pla, C.; Benavente, D. Estimation of the Radon Risk Under Different European Climates and Soil Textures. *Front. Public Health* **2022**, *10*, 794557. [CrossRef] [PubMed]
79. Leshukov, T.; Legoshchin, K.; Savkina, M.; Baranova, E.; Avdeev, K.; Larionov, A. Spatial Variations of Physical Characteristics of Soil and Their Role in Creating a Model of a Geogenic Radon Hazard Index (GRHI) in the Kuznetsk Coal Basin. *GeoHazards* **2024**, *5*, 1294–1307. [CrossRef]
80. Dueñas, C.; Pérez, M.; Fernández, M.C.; Carretero, J. Radon Concentrations in Surface Air and Vertical Atmospheric Stability of the Lower Atmosphere. *J. Environ. Radioact.* **1996**, *31*, 87–102. [CrossRef]
81. Nunes, L.J.R.; Curado, A.; Lopes, S.I. The Relationship between Radon and Geology: Sources, Transport and Indoor Accumulation. *Appl. Sci.* **2023**, *13*, 7460. [CrossRef]
82. Kashif, M.; Cao, Y.; Yuan, G.; Asif, M.; Javed, K.; Mendez, J.N.; Khan, D.; Miruo, L. Pore Size Distribution, Their Geometry and Connectivity in Deeply Buried Paleogene Es1 Sandstone Reservoir, Nanpu Sag, East China. *Pet. Sci.* **2019**, *16*, 981–1000. [CrossRef]
83. Etiope, G.; Klusman, R.W. Geologic Emissions of Methane to the Atmosphere. *Chemosphere* **2002**, *49*, 777–789. [CrossRef] [PubMed]
84. Chen, Z.; Li, Y.; Liu, Z.; Lu, C.; Zhao, Y.; Wang, J. Evidence of Multiple Sources of Soil Gas in the Tangshan Fault Zone, North China. *Geofluids* **2019**, *2019*, 1945450. [CrossRef]
85. Fiehn, A.; Eckl, M.; Kostinek, J.; Gałkowski, M.; Gerbig, C.; Rothe, M.; Röckmann, T.; Menoud, M.; Maazallahi, H.; Schmidt, M.; et al. Source Apportionment of Methane Emissions from the Upper Silesian Coal Basin Using Isotopic Signatures. *Atmos. Chem. Phys.* **2023**, *23*, 15749–15765. [CrossRef]
86. Miklyaev, P.; Petrova, T.; Tsapalov, A.; Borisov, A. Application Experience the Isotop Geochemical Method to Study the Condition of Radon Migration to the Soil Surface. *ANRI* **2021**, *1*, 15–21.